Finite Element Analysis of GTAW Welding Arc Based on Rotational Arc Sensor

Jianping Jia[1(✉)], Xin Wang[1], Shuhao Jia[2], Jigang Liu[1], and Shixiong Ai[1]

[1] School of Mechatronics Engineering, Nanchang University, No. 999 Xuefu Ave, Nanchang 330031, China
jpjia@ncu.edu.cn

[2] College of Precision Instrument and Opto-Electronics Engineering, Tianjin University, Tianjin 300072, China

Abstract. A three-dimensional mathematical model of rotational gas tungsten arc welding (GTAW) was established according to magnetohydrodynamics (MHD) theory, the welding arc of conventional GTAW and rotational GTAW were simulated by FLUENT to get the arc plasma's temperature field, velocity field and the static pressure field. The results show that the centrifugal force has little influence on the arc plasma because it's far weaker than the electromagnetic force, and the arc shape as well as physical quantity distribution of these two kinds of welding methods are essentially consistent.

Keywords: Rotational GTAW · Welding arc · FLUENT · Numerical simulation

1 Introduction

GTAW process has been widely used in industrial welding applications [1–6]. Rotational GTAW welding is a promising welding method. This method not only has the advantages of conventional GTAW welding but also the rotational arc sensor that can realize seam tracking and welding automation. Rotational arc sensor can avoid the effects of arc light, high temperature and high magnetic field. The sensor and arc are unified whole, so the sensor has good real-time performance and tracking effect as the arc voltage is sensing signal. Rotational arc sensor has compact structure and low cost, mainly apply to arc welding robot and cross slider. Stable arc can obtain good surface appearance and excellent internal quality. Rotational GTAW welding plasma is subjected to centrifugal force which may affect the arc plasma basic phenomenon. Because of the particularity of rotational GTAW welding, stable arc is the premise of seam tracking and welding automation. So, it is important and useful to understand the basic phenomena in arc plasma. But, it is very difficult to clarify these phenomena experimentally [4, 7, 8]. Due to the rapid development of computer technology, it promoted a deeper understanding of arc plasma by Numerical Simulation. Many studies pay attention to numerical simulation of conventional GTAW welding arc [9–13], but not to rotational GTAW welding arc. In order to provide more theory evidence of application in practical production by using rotational arc sensor, this paper did some research about rotational GTAW with the help of commercial CFD software FLUENT.

S. Chen et al. (eds.), *Transactions on Intelligent Welding Manufacturing*,
Transactions on Intelligent Welding Manufacturing, DOI 10.1007/978-981-10-5355-9_12

Mathematical model been established based on MHD theory and physical prototype. Due to the large temperature variation range in arc zone, and the thermal physical parameters of Ar present highly nonlinear variation in different temperature. Those parameters have great influence on current density distribution, electric potential distribution, temperature field distribution, arc formation and stability. In addition, the current continuity equation is added by UDS (User Define Scalar), and the current density equation is obtained. Using the redevelopment technology of FLUENT based on UDF to connect the physical parameters of argon at high temperature to the mathematical model. Conventional GTAW welding arc and rotational GTAW welding arc have been simulated separately, and the comparative analysis has also been made. Arc temperature field, velocity field and plasma pressure field of rotational GTAW welding not only have great influence on welding process, melting efficiency and melting pool behavior but also can provide basic data of investigation on arc stability. A high-speed camera platform was built, and the arc shapes of those two kinds of welding methods are compared. Because the other physical field of arc plasma is difficult to experimentally verified, and arc shape have close relationship with arc temperature field [14]. So, only the experiment to verify whether rotational arc will have great influence on arc shape been experimentalized.

2 Establishing the Physical Model

GTAW welding arc system which is based on rotational arc sensor (0–40 Hz) was taken as physical prototype to establish mathematical model. The physical prototype is shown in Fig. 1. Tungsten electrode sticks out from ceramic nozzle, and doesn't rotate itself. When tungsten electrode revolves around central axis, GTAW welding arc will be driven to revolve too. Argon was used as protective atmosphere. Because the asymmetry and the centrifugal force during Tungsten electrode's revolution process, it is necessary to use three-dimensional mathematical model to simplify the physical prototype. Mathematical model is shown in Fig. 2.

Fig. 1. Physical prototype of rotational arc sensor

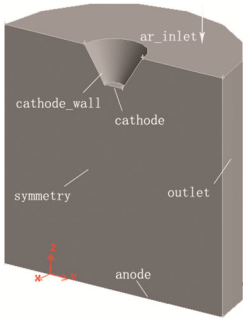

Fig. 2. Simplified mathematical model

This model's cathode is tungsten and anode is workpiece. Tungsten's diameter is 3.2 mm, cone angle is 60°, and it revolves around Z axis. The distance between tungsten's axis and Z axis is 2 mm, which means revolving radius is 2 mm. The distance between the end of the tungsten and anode, is 10 mm that means arc length is 10 mm.

3 Governing Equations

Several basic hypothesis have been made during calculation process: (1) arc plasma is incompressible continuous fluid; (2) arc plasma is in local thermal equilibrium (LTE) state; (3) arc plasma is optically thin, and it's flow state is laminar flow; (4) protective atmosphere is pure argon, and it's physical parameters change with temperature; (5) the effects of the electrode sheath can be ignored.

Based on the above hypotheses, incompressible fluid's Navier Stokes equations under three-dimensional Cartesian coordinate system and Maxwell's electromagnetic equations were chosen as the basic equations of arc simulation.

Fluid's continuity equation:

$$\frac{\partial u}{\partial x}+\frac{\partial v}{\partial y}+\frac{\partial w}{\partial z}=0 \tag{1}$$

X, Y, Z direction's momentum conservation equation:

$$\rho\left(u\frac{\partial u}{\partial x}+v\frac{\partial u}{\partial y}+w\frac{\partial u}{\partial z}\right)=\frac{\partial}{\partial x}\left(\mu\frac{\partial u}{\partial x}\right)+\frac{\partial}{\partial y}\left(\mu\frac{\partial u}{\partial y}\right)+\frac{\partial}{\partial z}\left(\mu\frac{\partial u}{\partial z}\right)-\frac{\partial P}{\partial x}+S_x \tag{2}$$

$$\rho\left(u\frac{\partial v}{\partial x}+v\frac{\partial v}{\partial y}+w\frac{\partial v}{\partial z}\right)=\frac{\partial}{\partial x}\left(\mu\frac{\partial v}{\partial x}\right)+\frac{\partial}{\partial y}\left(\mu\frac{\partial v}{\partial y}\right)+\frac{\partial}{\partial z}\left(\mu\frac{\partial v}{\partial z}\right)-\frac{\partial P}{\partial y}+S_y \tag{3}$$

$$\rho\left(u\frac{\partial w}{\partial x}+v\frac{\partial w}{\partial y}+w\frac{\partial w}{\partial z}\right)=\frac{\partial}{\partial x}\left(\mu\frac{\partial w}{\partial x}\right)+\frac{\partial}{\partial y}\left(\mu\frac{\partial w}{\partial y}\right)+\frac{\partial}{\partial z}\left(\mu\frac{\partial w}{\partial z}\right)-\frac{\partial P}{\partial z}+S_z \tag{4}$$

Energy conservation equation:

$$\rho C_P\left(u\frac{\partial T}{\partial x}+v\frac{\partial T}{\partial y}+w\frac{\partial T}{\partial z}\right)=\frac{\partial}{\partial x}\left(k\frac{\partial T}{\partial x}\right)+\frac{\partial}{\partial y}\left(k\frac{\partial T}{\partial y}\right)+\frac{\partial}{\partial z}\left(k\frac{\partial T}{\partial z}\right)+S_H \tag{5}$$

$$S_H=\frac{j_x^2+j_y^2+j_z^2}{\sigma}+\frac{5k_B}{2e}\left(j_x\frac{\partial T}{\partial x}+j_y\frac{\partial T}{\partial y}+j_z\frac{\partial T}{\partial z}\right)-S_R \tag{6}$$

where ρ is fluid density; u, v, w are the velocity of x, y, z direction respectively; μ is dynamic viscosity coefficient; Sx, Sy, Sz are momentum equation's source terms of x, y, z direction respectively; T, Cp, k are temperature, heat capacity at constant pressure, thermal conductivity respectively; j_x, $_{jy}$, j_z are current density of x, y, z direction respectively; σ is electrical conductivity; k_B is the Boltzmann constant; e is electronic power; S_R is radiation heat loss; S_H is the source term of energy equation. The three items on the right of formula 6 represent Joule heat, electron heat and radiation energy loss

respectively. Current density can be calculated by current continuity equation and Ohms law.

Current continuity equation:

$$\frac{\partial}{\partial x}(\sigma\frac{\partial\varphi}{\partial x})+\frac{\partial}{\partial y}(\sigma\frac{\partial\varphi}{\partial y})+\frac{\partial}{\partial z}(\sigma\frac{\partial\varphi}{\partial z}) \tag{7}$$

Ohms law:

$$j_x=\sigma\frac{\partial\varphi}{\partial x},j_y=\sigma\frac{\partial\varphi}{\partial y},j_z=\sigma\frac{\partial\varphi}{\partial z} \tag{8}$$

where φ is scalar potential; μ_0 is magnetic medium constant; j_x, j_y, j_z represent current density of x, y, z direction respectively.

Magnetic induction intensity can be calculated by introducing magnetic vector potential. The components of x, y, z directions respectively are:

$$B_x=\frac{\partial A_z}{\partial y}-\frac{\partial A_y}{\partial z};B_y=\frac{\partial A_x}{\partial z}-\frac{\partial A_z}{\partial x};B_z=\frac{\partial A_y}{\partial x}-\frac{\partial A_x}{\partial y} \tag{9}$$

Momentum equation's source terms are composed of the following equations:

$$S_x=j_yB_z-j_zB_y+F_{lx};S_y=j_zB_x-j_xB_z+F_{ly};S_z=j_xB_y-j_yB_x-\rho g \tag{10}$$

where F_{lx}, F_{ly} are the components of centrifugal force on x, y directions, source terms were added by UDF to FLUENT solver [15].

Rotational GTAW welding arc are influenced by centrifugal force, and the formula of centrifugal force is:

$$F_l=mr\omega^2 \tag{11}$$

where m is plasma's mass; r is radius of gyration; ω is rotation frequency. When centrifugal force is loaded as source term, it must firstly be transformed into body component force of x, y directions.

4 Model Construction and Mesh Generation

Based on the above mathematical model, using GAMBIT that is pre-processing software of ANSYS to establish for 3D geometric modeling and generate mesh of the mathematical model. GAMBIT software is simple to operate, flexible and convenient, as well as has a strong ability for mesh generation. The special mesh generation algorithm can directly divide the complex geometrical area into high quality tetrahedron, hexahedron and hybrid grid [16].

Conventional GTAW welding arc and rotational GTAW welding arc share a mathematical model, the difference between two welding process is whether to load centrifugal force source term. In order to improve the mesh quality, those two mesh models

all use good accuracy hexahedral mesh, including wedge mesh in suitable positions. Mesh model is shown in Fig. 3. For the regions with large related physical quantity gradient, self-adaptive mesh refinement functions in FLUENT can be used for local refinement.

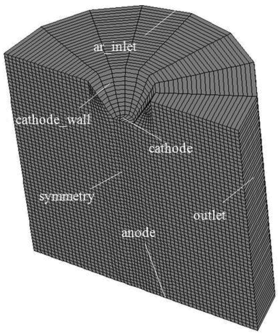

Fig. 3. Mesh model

After modeling and meshing, the boundary type of this model in GAMBIT was set. Among them,cathode_wall, anode and cathode were setup as no slip wall, namely there are no loss of material and energy on these walls. ar_inlet was setup as velocity-inlet boundary condition, outlet was setup as pressure-outlet boundary condition, and symmetry was setup as symmetry plane boundary condition.

5 Setting of the Boundary Conditions

In this paper, boundary conditions were set up according to the actual situation and the previous assumptions. Boundary conditions are shown in Table 1. In Table 1, v_{giv} represents inflow rate of protective gas. Argon thermodynamic parameters, such as density, viscosity, conductivity, specific heat capacity and thermal conductivity in this paper come from the literature [17].

Table 1. Setting of the boundary conditions

Boundary name	Boundary type	$\boldsymbol{V}$	T	φ	$\boldsymbol{A}$
ar_inlet	velocity inlet	$v_z = v_{giv}$	1000	$\partial\varphi/\partial n = 0$	$\partial A/\partial n = 0$
cathode_wall	wall	0	1000	$\partial\varphi/\partial n = 0$	$\partial A/\partial n = 0$
cathode	wall	0	3000	$-\sigma \cdot \partial\varphi/\partial z = I/(\pi r^2)(r < 0.5)$	$\partial A/\partial n = 0$
outlet	presure outlet	$\partial V/\partial n = 0$	1000	$\partial\varphi/\partial n = 0$	0
symmetry	symmetry	$\partial V/\partial x = 0$	$\partial T/\partial x = 0$	$\partial\varphi/\partial x = 0$	$\partial A/\partial n = 0$
anode	wall	0	5000	0	$\partial A/\partial n = 0$

6 Simulation Results and Analysis

After completing the above related settings, the model was introduced into FLUENT to calculate for solution. In this paper, numerical simulation of conventional GTAW welding arc and rotational GTAW welding arc were carried out respectively with welding current 200 A. The welding current polarity is straight polarity direct current. Rotational frequency of rotational GTAW welding arc is 40 Hz, and the direction is counter clockwise. Iterative calculation was carried out based on SIMPLE (semi-implicit method for pressure-linked equations) [18] algorithm in the FLUENT until convergence.

Since the arc plasma can only keep local thermal equilibrium when the temperature is above 10000 K [19], Fig. 4 shows the comparison between experimental and simulation temperature contours in rotational GTAW welding arc above 10000 K. As can be seen from Fig. 4, arc temperature field shows bell shaped, and in the two electrodes temperature gradient is bigger. Furthermore, the highest temperature appears near cathode. Arc temperature reaches the maximum value near cathode. The reason for this phenomenon is that maximum current density in the end of tungsten electrode induced maximum heat production, and tungsten emission electron has a cooling effect on it. So the highest temperature doesn't appear on tungsten electrode. It's difficult to measure arc temperature under high temperature gradient. So, experimental value that has already been made is used for comparing with simulations value, and those two shapes of contour are basically the same. The experiment results (200 A at 10-mm arc length) come from Hsu et al. [20]. Figure 5 shows the distribution map of arc temperature distribution of tungsten electrode axis in two different welding modes. From the diagram, the temperature distribution on the axis of two welding modes is basically same.

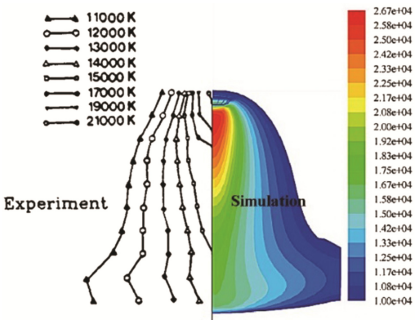

Fig. 4. Comparison between experimental and simulation temperature contours in rotational GTAW welding

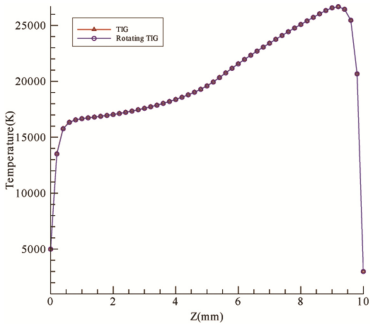

Fig. 5. Arc temperature distribution of tungsten electrode axis

Figure 6 is the velocity field distribution cloud picture of arc plasma in rotational GTAW welding arc. The pressure difference between two electrodes induced plasma fluid force, so the plasma in Fig. 6 flows from cathode to anode at a high speed. The velocity of plasma near cathode is faster, which is due to the larger current density near cathode leads to a larger plasma fluid force and a large force on the plasma of this zone. The velocity of arc plasma reaches maximum under the influence of plasma flow force, and then decreases with the barrier of workpiece. Figure 7 shows the velocity distribution curve of conventional GTAW welding and rotational GTAW welding on the axis of tungsten electrode. The integrated speed of conventional GTAW welding on the axis of tungsten electrode is slightly higher than that of the rotational GTAW welding. The reason is that plasma of rotational GTAW welding is subjected to centrifugal force but the conventional GTAW welding not, so the plasma of rotational GTAW welding tends to be spun off. What's more, the integrated speed of rotational GTAW welding on the tungsten electrode axis is slightly lower, but the velocity fields of those two different welding modes don't have much difference, and can be regarded as the same.

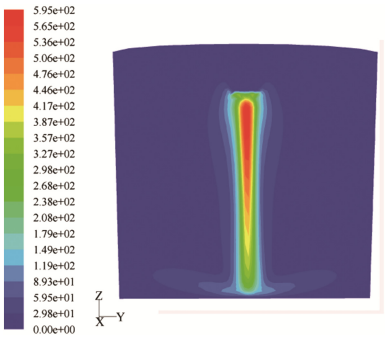

Fig. 6. Velocity field of rotational GTAW welding arc

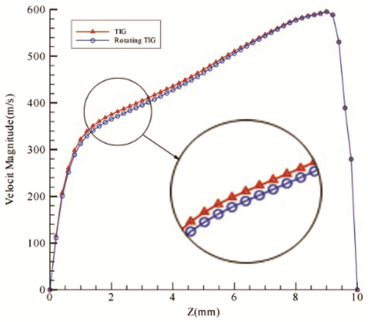

Fig. 7. Velocity distribution of tungsten electrode axis

Figure 8 shows the distribution cloud picture of arc plasma pressure field in rotational GTAW welding. The arc pressure is higher in anode and cathode zones, and decreases with the distance from two electrodes in arc column region. The reason of great pressure in cathode region is that the large gradient of current density in this zone caused the large electromagnetic pinch force. The large pressure in the anode region is mainly caused by the plasma rush to the workpiece at a high velocity. Figure 9 shows distribution curve of arc pressure on the surface of workpiece with conventional GTAW welding and rotational GTAW welding, From the diagram, it can be seen that the distribution curve of two different welding modes are basically in coincidence. Because of plasma velocity on the surface of workpiece decreases with the distance away from the axis ($y = 2$ mm) of tungsten electrode, the arc pressure of two different welding modes are all double exponential distribution.

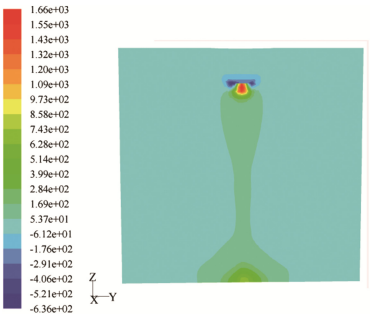

Fig. 8. Pressure field of rotational GTAW welding arc

The arc temperature field, velocity field and plasma pressure field distribution cloud picture of these two different welding modes are compared, it can be seen that the conventional GTAW welding is basically the same with rotational GTAW welding. The reason of this phenomenon is that the centrifugal force is much smaller than the electromagnetic force when rotational frequency is 40 Hz (the maximum frequency of the rotational arc sensor). The highest temperature, the biggest velocity of plasma, the

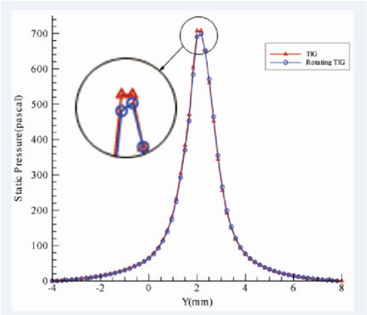

Fig. 9. Pressure distribution of workpiece surface

biggest arc pressure and the gradient of those physical quantity all appears near cathode. It shows that there is a correlation between those three physical quantity.

On the *YZ* plane of rotational GTAW welding, the centrifugal force distribution from the end of tungsten to workpiece along *Y* axis is shown in Fig. 10. On this curve, centrifugal force increases with the distance away from the axis of revolution, but the maximum value is only 238 N/m^3, which can almost be neglected compared with the electromagnetic pinch force(105 N/m^3). It can be concluded that the arc shape and the related physical quantities in rotational GTAW welding within rotational frequency range is basically the same as conventional GTAW welding.

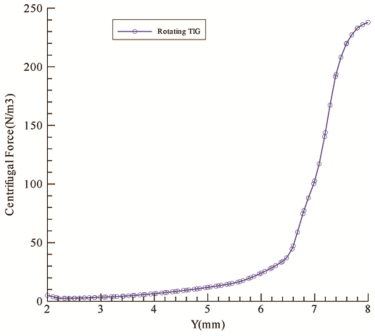

Fig. 10. Centrifugal force distribution along *Y* axis

7 Experimental Verification

However, it is difficult to monitor arc temperature field, velocity field and plasma pressure field, because GTAW welding arc is an instantaneous physical process at high temperature. The strong arc light also causes interference. There is a close relationship between the arc shape and arc temperature field distribution [14]. So, the arc shape is obtained by high-speed camera system to verify the above conclusions. High-speed camera shooting frame count is 500 frame/s. Conventional GTAW welding arc and

rotational GTAW welding arc which rotational frequency is 16 Hz were photographed respectively. GTAW welding arc shape are showed in Fig. 11. It can be learned from the graphs that both of them are bell shaped, and the simulation results are reliable.

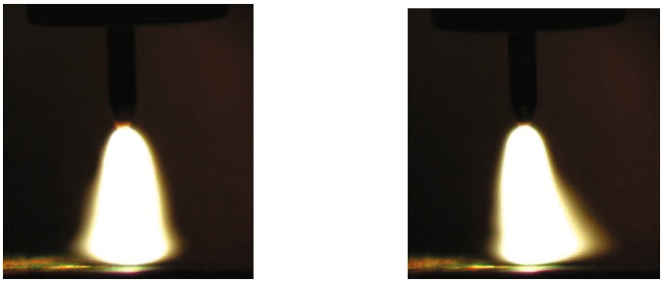

(a) Conventional GTAW welding arc (b) Rotational GTAW welding arc

Fig. 11. GTAW welding arc shape

8 Conclusions

(1) Mathematical model of rotational GTAW welding arc has been established based on MHD theory. Numerical simulation of rotational GTAW welding arc was carried out with the welding current of 200 A and the rotational frequency is 40 Hz. Arc temperature field, velocity field and plasma pressure field distribution cloud picture were obtained.

(2) In order to compare and analyze, the conventional GTAW welding arc has also been simulated. Arc temperature field, velocity field and plasma pressure field of the two different welding modes are basically the same. The reason of this phenomenon is that centrifugal force is far less than electromagnetic pinch force. So, centrifugal force can almost be neglected.

Acknowledgement. The research is supported by the province science and technology of Jiangxi offend pass item (20142BBE50062). Innovative fund for graduate students of Nanchang University (cx2016075).

References

1. Murphy AB, Tanaka M, Tashiro S et al (2009) A computational investigation of the effectiveness of different shielding gas mixtures for arc welding. J Phys D Appl Phys 42(11): 115205
2. Lu S, Dong W, Li D et al (2009) Numerical study and comparisons of gas tungsten arc properties between argon and nitrogen. Comput Mater Sci 45(2):327–335
3. Lago F, Gonzalez JJ, Freton P et al (2004) A numerical modelling of an electric arc and its interaction with the anode. Part I. The two-dimensional model. J Phys D Appl Phys 37(6):883
4. Savaş A, Ceyhun V (2012) Finite element analysis of GTAW arc under different shielding gases. Comput Mater Sci 51(1):53–71

5. Traidia A, Roger F, Chidley A et al (2011) Effect of helium-argon mixtures on the heat transfer and fluid flow in gas tungsten arc welding. World Acad Sci Eng Technol 73:854–861
6. Tashiro S, Tanaka M, Ushio M et al (2006) Prediction of energy source properties of free-burning arcs. Vacuum 80(11–12):1190–1194
7. Lu F, Yao S, Lou S et al (2004) Modeling and finite element analysis on GTAW arc and weld pool. Comput Mater Sci 29(3):371–378
8. Tanaka M, Ushio M, Lowke JJ (2004) Numerical study of gas tungsten arc plasma with anode melting. Vacuum 73(3–4):381–389
9. Ding X, Li H, Yang L et al (2014) Numerical analysis of arc characteristics in two-electrode GTAW. Int J Adv Manuf Technol 70(9):1867–1874
10. Faraji AH, Goodarzi M, Seyedein SH et al (2014) Experimental study and numerical modeling of arc and weld pool in stationary GTA welding of pure aluminum. Int J Adv Manuf Technol 71(9):2059–2207
11. Shirvan AJ, Choquet I (2016) A review of cathode-arc coupling modeling in GTAW. Weld World 60(4):1–15
12. Luo J, Yao Z, Xue K (2016) Anti-gravity gradient unique arc behavior in the longitudinal electric magnetic field hybrid tungsten inert gas arc welding. Int J Adv Manuf Technol 84(1): 647–661
13. Kanemaru S, Sasaki T, Sato T et al (2014) Study for TIG–MIG hybrid welding process. Weld World Le Soudage Dans Le Monde 58(1):11–18
14. Chen QW, Hu TS, Xu YT (1986) Welding arc shape and arc temperature field. J Beijing Aeronaut Astronaut Inst 03:7–16
15. Inc Fluent (2014) FLUENT user's guide. Fluent Inc., Lebanon
16. Inc Fluent (2003) GAMBIT modeling guide. Fluent Inc., Lebanon
17. Choo RTC, Szekely J, Westhoff RC (1992) On the calculation of the free surface temperature of gas-tungsten-arc weld pools from first principles. part I. modeling the welding arc. Metall Mater Trans B 23B(6):357–369
18. Barakos G, Mitsoulis E, Assimacopoulos D (1994) Natural convection flow in a square cavity revisited: laminar and turbulent models with wall functions. Int J Num Methods Fluids 18(7): 695–719
19. Li HX (2011) Numerical analysis on keyhole gas tungsten arc welding. Dissertation, Lanzhou University of Technology, China
20. Hsu KC, Etemadi K, Pfender E (1983) Study of the free-burning high-intensity argon arc. J Appl Phys 54(3):1293–1301